# The Pressure Induced $B1$–$B2$ Phase Transition of CdO

P. Bhardwaj*
High Pressure Research Lab., Department of Physics, Barkatullah University, Bhopal-462026, India

*(Received August 8, 2012)*

In this paper, the structural, elastic and thermodynamic properties of CdO under different pressure range have been reported. An extended interaction potential model (including the zero point energy effect) has been used for this study. Phase transition pressures are associated with a sudden collapse in volume. At compressed volume, the present oxide is found in cesium chloride (CsCl) phase. The calculated second order elastic constants and their various combinations have been reported in different pressure range. The calculated values have been compared with available results. Our values have been found in good agreement with existing findings.

DOI: 10.12693/APhysPolA.124.677
PACS: 62.20.de, 62.20.dq, 62.50.−p

## 1. Introduction

The group-IV wide-gap semiconductor materials are very important because of their opto-electronic technological applications. They are used as commercial short wavelength light-emitting diodes, laser diode candidates by $p$-type doping with nitrogen, transparent conductors, solar cells, high-density optical memories, and visual displays. These properties arise because of the role of $d$-electrons in the valence band in hybridization [1–3]. Many researchers have focused on a cadmium oxides (CdO) because of a wide range of technical applications for example as transparent electrodes, display devices, sensors, diodes, gas sensors etc. These uses of CdO stand on its specific optical and electrical properties [4]. Cadmium oxide is an $n$-type semiconductor that crystallizes in rock-salt structure at normal conditions. It presents an optical band gap of about 2.3 eV, with an indirect band gap of 1.36 eV [5].

The phase transition pressure of CdO from NaCl ($B1$) to CsCl ($B2$) has been studied at 85 GPa, by Schleife et al. [6] and 515 GPa by Jaffe et al. [7]. The experimental research on the compressibility and phase transition of CdO up to 176 GPa at room temperature using high-resolution angular-dispersive X-ray diffraction from synchrotron source combined with the diamond anvil cell technique have been studied by Liu et al. [8]. The phase transition from NaCl ($B1$) to CsCl ($B2$)-type structure for CdO was observed at pressure about 90.6 GPa by them. The bulk modulus and equilibrium lattice parameter were estimated by fitting the energy as a function of volume according the Murnagham equation of state (EOS) [9]. Guerrero-Moreno and Takeuchi [10] have studied the NaCl ($B1$) to CsCl ($B2$) structural phase transition of CdO at about 89–91 GPa range. Peng et al. [11] have predicted the pressure dependent Poisson ratio, Debye temperature and shear elastic wave velocities using plane wave pseudopotential method.

Recently, Dakhel et al. [12] studied the electrical and optical properties, transparent conducting properties, band-gap narrowing from various doping with CdO like iron-doped CdO, samarium-doped CdO, dysprosium-doped CdO and europium-doped CdO. The first-principles calculations of the elastic and thermodynamic properties for CdO in both the $B1$ (rocksalt) phase and $B2$ (cesium chloride) phase have been performed within the framework of density functional theory, using the pseudopotential plane-wave method by Li et al. [13]. X-ray structure factors and Compton profiles of CdO are presented by Dhaka et al. [14]. They also performed the theoretical calculations employing the first-principles linear combination of atomic orbitals (LCAO) method using the CRYSTAL code. First-principles calculations of the crystal structures, and phase transition, and elastic properties of cadmium oxide (CdO) have been carried out with the plane-wave pseudopotential density functional theory method by Peng et al. [15]. Li et al. [13] committed that, however, the accuracy of the predicted phase transition pressure, which was determined from the overlap of the energy-volume curves of $B1$ and $B2$ phases, is somewhat questionable. The several factors altering such predictions are the relativistic correction, nonzero temperature, and zero-point motion effect not being included in these calculations. Thus, accurate diffraction measurements for CdO were performed in order to check the validity of the theoretically predicted high pressure phase transition.

Seeing at the interesting properties of this less explored CdO and the fact that no work has been done with the potential model including zero point energy effects, the extended interaction potential (EIP) model has been applied, which includes the zero point energy effect in the potential model. In the present model three-body interactions forces have been included. It is seen from the current literature that three-body potential (TBP) model has been found to be remarkably successful in giving the unified description of structural and elastic properties of ionic and semiconducting crystals [16–23]. In this TBP model, the three-body interactions owe their origin to

*e-mail: purveebhardwaj@gmail.com

the quantum mechanical foundation and also to the phenomenological approach [24, 25] in terms of the transfer (or exchange) of charge between the overlapping electron shells of the adjacent ions in solids. This TBP approach has been extended to include the Hafemeister–Flygare (HF) type [26] overlap repulsion operative up to the second neighbour ions for describing, the lattice static and mechanical properties of binary ionic solids and alloys. Also, Tosi and Fumi [27] have demonstrated the significance of van der Waals (VDW) attraction due to the dipole–dipole (d–d) and dipole–quadrupole (d–q) interactions to describe the cohesion in ionic solids and they are generally ignored in the first principle calculations. This model is also able to explain the Cauchy violation ($C_{12} \neq C_{44}$) in the second order elastic constants while two-body potential model could not explain this violation.

An extended interaction potential model has been applied by including zero point energy effects in TBP for the prediction of phase transition pressures and associated volume collapses in calcium oxide. The zero point energy is the ground state energy of the compound. This term shows a small effect in the Gibbs free energy but to make model realistic it cannot be ignored completely. The purpose of this work is to provide an improved model suitable for the study of structural, elastic, thermophysical and thermodynamic properties of cadmium oxide. The rest of this paper is organized as follows: the method of calculation is given in Sect. 2, the results and conclusion are presented and discussed in Sect. 3.

## 2. Potential model and method of calculation

Application of pressure directly results in compression leading to the increased charge transfer (or three-body interaction effect [28]) due to the deformation of the overlapping electron shell of the adjacent ions (or non-rigidity of ions) in solids. Also we have considered zero point energy effects, which is the lowest possible energy that the compound may possess. The energy of the compound is $\varepsilon = h\nu/(\mathrm{e}^{h\nu/kt} - 1) + h\nu/2$, here $\nu$, $h$, $t$, and $k$ are the frequency, Planck constant, temperature and Boltzmann constant of the compound. It is clear from the above expression that even at absolute zero the energy of the compound cannot be zero but at least $h\nu/2$. Hence there arises a need to include the zero point energy term in TBP approach for better agreement with experimental approaches.

These effects have been incorporated in the Gibbs free energy ($G = U + PV - TS$) as a function of pressure and three-body interactions (TBI) [28], which are the most dominant among the many-body interactions. Here, $U$ is the internal energy of the system equivalent to the lattice energy at temperature near zero and $S$ is the entropy. At temperature $T = 0$ K and pressure ($P$) the Gibbs free energies for rock salt ($B1$, real) and CsCl ($B2$, hypothetical) structures are given by

$$G_{B1}(r) = U_{B1}(r) + PV_{B1}(r), \tag{1}$$

$$G_{B2}(r') = U_{B2}(r') + PV_{B2}(r'), \tag{2}$$

with $V_{B1}$ ($= 2.00r^3$) and $V_{B2}$ ($= 1.54r'^3$) as unit cell volumes for $B1$ and $B2$ phases, respectively. The first terms in (1) and (2) are lattice energies for $B1$ and $B2$ structures and they are expressed as

$$\begin{aligned} U_{B1}(r) = {} & \frac{-\alpha_{\mathrm{m}} Z^2 e^2}{r} - \frac{12\alpha_{\mathrm{m}} Z e^2 f_(r)}{r} - \left(\frac{C}{r^6} + \frac{D}{r^8}\right) \\ & + 6b\beta_{ij} \exp\left((r_i + r_j - r)/\rho\right) \\ & + 6b\beta_{ii} \exp\left((2r_i - 1.414r)/\rho\right) \\ & + 6b\beta_{jj} \exp\left((2r_j - 1.414r)/\rho\right) + 0.5h \left\langle \omega^2 \right\rangle_{B1}^{1/2}, \end{aligned} \tag{3}$$

$$\begin{aligned} U_{B2}(r') = {} & \frac{-\alpha'_{\mathrm{m}} Z^2 e^2}{r'} - \frac{16\alpha'_{\mathrm{m}} Z e^2 f(r')}{r'} - \left(\frac{C'}{r'^6} + \frac{D'}{r'^8}\right) \\ & + 8b\beta_{ij} \exp\left((r_i + r_j - r')/\rho\right) \\ & + 3b\beta_{ii} \exp\left((2r_i - 1.154r')/\rho\right) \\ & + 3b\beta_{jj} \exp\left((2r_j - 1.154r')/\rho\right) + 0.5h \left\langle \omega^2 \right\rangle_{B_2}^{1/2}, \end{aligned} \tag{4}$$

with $\alpha_{\mathrm{m}}$ and $\alpha'_{\mathrm{m}}$ as the Madelung constants for NaCl and CsCl structure, respectively. $C$ ($C'$) and $D$ ($D'$) are the overall VDW coefficients of $B1$ ($B2$) phases, $\beta_{ij}$ ($i, j = 1, 2$) are the Pauling coefficients. $Ze$ is the ionic charge and $b$ ($\rho$) are the hardness (range) parameters, $r$ ($r'$) are the nearest neighbour separations for NaCl (CsCl) structure, $f(r)$ is the three-body force parameter.

The term $\langle \omega^2 \rangle^{1/2}$ as the mean square frequency related to the Debye temperature ($\theta_{\mathrm{D}}$) as

$$\langle \omega^2 \rangle^{1/2} = k\theta_{\mathrm{D}}/h.$$

Here, $\theta_{\mathrm{D}}$ can be expressed as [29]:

$$\theta_{\mathrm{D}} = (h/k)[(5rB_{\mathrm{T}})/\mu]^{1/2},$$

with $B_{\mathrm{T}}$ and $\mu$ as the Bulk modulus and reduced mass of the compounds.

These lattice energies consist of long range Coulomb energy (first term), three-body interactions corresponding to the nearest neighbour separation $r$ ($r'$) (second term), VDW interaction (third term), energy due to the overlap repulsion represented by HF type potential and extended up to the second neighbour ions (fourth, fifth and sixth terms), and last term indicates zero point energy effect term.

## 3. Results and discussion

The Gibbs free energies contain three model parameters [$b$, $\rho$, $f(r)$]. The values of these parameters have been evaluated using the first and second order space derivatives of the cohesive energy ($U$) expressed as [19–23]:

$$\left[\frac{\mathrm{d}U}{\mathrm{d}r}\right]_{r=r_0} = 0, \tag{5}$$

$$\left[\frac{\mathrm{d}^2U}{\mathrm{d}r^2}\right]_{r=r_0} = 9kr_0B_{\mathrm{T}}. \tag{6}$$

Using these model parameters and the minimization tech-

nique, phase transition pressures of CdO has been computed. The input data of the crystal and calculated model parameters are listed in Table I.

TABLE I

Input parameters and generated model parameters for CdO.

| Solid | Input parameters | | Model parameters | | |
|---|---|---|---|---|---|
| | $r_0$ [Å] | $B$ [GPa] | $b$ [$10^{-12}$ erg] | $\rho$ [Å] | $f(r)$ |
| CdO | 2.389[a] | 148[a] | 14.70236 | 0.264 | 0.17402 |

[a] Ref. [8]

### *3.1. Structural properties*

The $B1$ (NaCl) structure is most stable in these compounds and at high pressure they transform to body centered $B2$ (CsCl) structure. As the stable phase is associated with minimum free energy of the crystal, we have followed the technique of minimization of the Gibbs free energies of real and hypothetical phases. We have minimized $G_{B1}(r)$ and $G_{B2}(r')$ given by Eqs. (3) and (4) at different pressures in order to obtain the interionic separations $r$ and $r'$ corresponding to $B1$ and $B2$ phases associated with minimum energies. The factor $\Delta G$ $[G_{B1}(r) \sim G_{B2}(r')]$ plays an important role in stability of structures. The phase transition occurs when $\Delta G$ approaches zero ($\Delta G \to 0$). The phase transition pressure ($P_t$) is the pressure at which $\Delta G$ approaches zero. At $P_t$ these compounds undergo a $B1$–$B2$ transition associated with a sudden collapse in volume showing a first order phase transition. Figure 1 shows present computed phase transition pressure for NaCl-type ($B1$) to CsCl-type ($B2$) structures in CdO at 91 GPa, while the experimental value is 90.6 GPa. The present phase transition pressure illustrated by arrows in Fig. 1 and its value have been listed in Table II and compared with their experimental [8] and other theoretical results [6, 7, 10, 11, 13, 15]. It is interesting to note from Table II and Fig. 1 that the phase transition pressures ($P_t$), obtained from the present model, are in general in closer agreement with experimental data [8] and match equally well with other theoretical results [6, 7, 10, 11, 13, 15].

TABLE II

Phase transition and volume change of CdO.

| Solid | Phase transition pressure [GPa] | | | Volume collapse [%] | |
|---|---|---|---|---|---|
| | present | expt. | others | present | others |
| CdO | 91 | 90.6[a] | 85[b], 515[c], 89–91[d], 102.5[e], 83.1[f], 90.31[g] | 6.3 | 6.5[g] |

[a] Ref. [3], [b] Ref. [6], [c] Ref. [7], [d] Ref. [10], [e] Ref. [15], [f] Ref. [11], [g] Ref. [13]

We have also computed the relative volume changes $V(P)/V(0)$ corresponding to the values of $r$ and $r'$ at different pressures and plotted them against the pressure in Fig. 2 for CdO. It is clear from Table II and Fig. 2 that our calculated volume collapses (%) from our present model for CdO is 6.3%, respectively. There is no available experimental value of volume collapse for CdO

TABLE III

Calculated values of elastic constants (in GPa), bulk modulus (in GPa), and anisotropy parameter and shear modulus (in GPa) of CdO.

| Solid | $C_{11}$ | $C_{12}$ | $C_{44}$ | $\mathrm{d}B/\mathrm{d}P$ | $\mathrm{d}S/\mathrm{d}P$ | $\mathrm{d}C_{44}/\mathrm{d}P$ |
|---|---|---|---|---|---|---|
| CdO | | | | | | |
| present | 192.68 | 99.87 | 51.46 | 4.065 | 0.426 | 0.371 |
| others | 183.99[a] | 96.01[a] | 45.78[a] | 4.91[a], 5[b], 4.71[c], 4.13[d] | – | – |
| expt. | – | – | – | 4[e] | – | – |

[a] Ref. [15], [b] Ref. [6], [c] Ref. [10], [d] Ref. [7], [e] Ref. [8]

TABLE IV

Calculated values of volume change, second order elastic constants and bulk modulus for CdO.

| $P$ | $V/V_0$ | $C_{11}$ | $C_{12}$ | $C_{44}$ | $B$ |
|---|---|---|---|---|---|
| 0 (present) | 1.00 | 192.68 | 99.87 | 51.46 | 130.80 |
| (others) | 1.00 | 183.99 | 96.01 | 45.78 | 125.34 |
| 10 (present) | 0.942 | 274.12 | 127.82 | 49.35 | 176.58 |
| (others) | 0.935 | 269.76 | 123.55 | 43.88 | 172.29 |
| 20 (present) | 0.896 | 358.05 | 151.79 | 47.21 | 220.54 |
| (others) | 0.888 | 352.24 | 148.84 | 41.20 | 216.64 |
| 30 (present) | 0.871 | 439.36 | 176.13 | 42.85 | 263.87 |
| (others) | 0.852 | 433.14 | 173.35 | 37.93 | 259.95 |
| 40 (present) | 0.837 | 516.97 | 199.76 | 39.11 | 305.49 |
| (others) | 0.822 | 511.31 | 196.53 | 34.31 | 301.45 |
| 50 (present) | 0.807 | 592.43 | 223.67 | 36.04 | 346.59 |
| (others) | 0.797 | 587.97 | 219.89 | 30.53 | 342.58 |
| 60 (present) | 0.789 | 668.12 | 247.18 | 31.45 | 387.49 |
| (others) | 0.775 | 662.58 | 242.64 | 26.34 | 382.62 |
| 70 (present) | 0.771 | 741.56 | 269.78 | 28.19 | 427.04 |
| (others) | 0.756 | 735.92 | 264.89 | 22.2 | 421.90 |
| 80 (present) | 0.762 | 815.24 | 292.37 | 23.44 | 466.66 |
| (others) | 0.739 | 808.49 | 287.05 | 17.74 | 460.86 |
| 90 (present) | 0.735 | 886.58 | 315.77 | 18.69 | 506.04 |
| (others) | 0.724 | 880.33 | 309.08 | 13.31 | 499.50 |
| 100 (present) | 0.723 | 957.31 | 336.81 | 13.47 | 543.64 |
| (others) | 0.710 | 951.16 | 330.86 | 8.81 | 537.63 |
| 110 (present) | 0.711 | 1027.72 | 358.29 | 9.76 | 581.43 |
| (others) | 0.697 | 1021.53 | 352.42 | 4.21 | 575.45 |
| 115 (present) | 0.702 | 1063.25 | 370.04 | 7.69 | 601.11 |
| (others) | 0.691 | 1057.13 | 363.08 | 1.85 | 594.43 |
| 116 (present) | 0.699 | 1071.32 | 372.07 | 6.66 | 605.15 |
| (others) | 0.690 | 1064.00 | 365.33 | 1.41 | 598.22 |
| 117 (present) | 0.698 | 1078.49 | 375.11 | 5.74 | 609.57 |
| (others) | 0.689 | 1070.92 | 367.39 | 0.93 | 601.90 |
| 118 (present) | 0.697 | 1085.64 | 377.89 | 4.98 | 613.80 |
| (others) | 0.688 | 1077.86 | 369.51 | 0.46 | 605.63 |
| 119 (present) | 0.696 | 1092.31 | 379.65 | 3.99 | 617.20 |
| (others) | 0.687 | 1084.74 | 371.58 | 0.01 | 609.30 |
| 120 (present) | 0.695 | 1099.16 | 381.45 | 3.25 | 620.68 |
| (others) | 0.686 | 1091.06 | 373.52 | −0.53 | 612.70 |
| 121 (present) | 0.694 | 1106.31 | 383.94 | 3.20 | 624.73 |
| (others) | 0.685 | 1098.43 | 375.77 | −0.99 | 616.65 |

Others — Ref. [15]

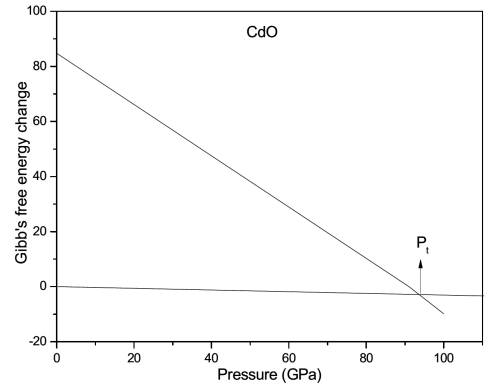


Fig. 1. Variation of $\Delta G$ (kJ/mol) with pressure for CdO.

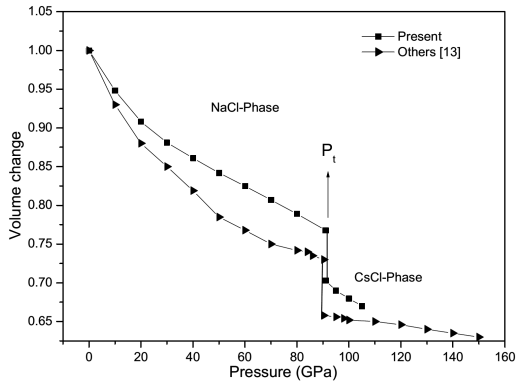


Fig. 2. Variation of volume change $V/V_0$ with pressure.

so we could not compare our results. Present results have been compared with density functional theory, using the pseudopotential plane-wave method by Li et al. [13]. It is obvious from Fig. 2 that the compression curve shows the same trend as reported by others [13]. The values of relative volume changes have also been calculated at different pressures. The comparisons of these values with plane--wave pseudopotential density functional theory method [15] have been given in Table IV. Present results are close as reported by Peng et al. [15].

### *3.2. Elastic properties*

The lattice theoretical study of second order elastic constants of cubic crystals has been applied by the method of homogeneous finite deformation. The knowledge of second order elastic constants (SOEC's) and their pressure derivatives are important for the understanding of the interatomic force in solids.

The expressions of SOEC's are as follows:

$$C_{11} = (e^2/4a^4)\big[-5.112Z(Z+12f(r)) + A_1 + (A_2+B_2)/2 + 9.3204zaf'(r)\big], \quad (7)$$

$$C_{12} = (e^2/4a^4)\big[0.226Z(Z+12f(r)) - B_1 + (A_2-5B_2)/4 + 9.3204zaf'(r)\big], \quad (8)$$

$$C_{44} = (e^2/4a^4)\big[2.556Z(Z+12f(r)) - B_1 + (A_2+3B_2)/4\big]. \quad (9)$$

Using model parameters ($b$, $\rho$, $f(r)$), pressure derivatives of SOEC's have been computed whose expressions are as follows:

$$\frac{\mathrm{d}B}{\mathrm{d}p} = -(3\Omega)^{-1}\big[13.980Z(Z+12f(r)) + C_1 - 3A_1 + C_2 - 3A_2 - 167.7648zaf'(r) + 41.9420za^2f(r)\big], \quad (10)$$

$$\frac{\mathrm{d}S}{\mathrm{d}p} = -(2\Omega)^{-1}\big[23.682Z(Z+12f(r)) + C_1 + (C_2+6A_2-6B_2)/4 - 50.0752zaf'(r) + 13.9808za^2f(r)\big], \quad (11)$$

$$\frac{\mathrm{d}C_{44}}{\mathrm{d}p} = -(\Omega)^{-1}\left[-11.389Z(Z+12f(r)) + A_1 - 3B_1 + \frac{C_2+2A_2-10B_2}{4}{}_1 + 44.6528Zaf'(r)\right], \quad (12)$$

$$B = \frac{1}{3}(C_{11}+2C_{12}), \quad S = \frac{1}{2}(C_{11}-C_{12})$$

and

$$\Omega = -2.330Z(Z+12f(r)) + A_1 + A_2 + 21.9612zaf'(r).$$

The values of $A_i$, $B_i$, and $C_i$ ($i = 1, 2$) have been evaluated from the knowledge of $b$, $\rho$ and VdW coefficients.

The study of elastic behaviour under pressure is well known to provide useful information about change in the nature of the covalent and ionic forces induced in the crystal as it is subjected to the phase transformation. The calculated values of SOEC's and their pressure derivatives have been given at $P = 0$ GPa in Table III. Our results have been compared with available experimental [8] and theoretical results [6, 7, 10, 15]. Experimental data are only available for pressure derivative of bulk modulus.

Furthermore the SOEC's and bulk modulus have been calculated at different pressure range 0–121 GPa and summarized in Table IV. Our calculated values of SOEC's and bulk modulus have been compared with the plane-wave pseudopotential density functional theory method by Peng et al. [15] throughout the pressure range. It is clear from this table that our calculated values demonstrate the same trend as reported by plane-wave pseudopotential density functional theory method [15]. These SOEC's and bulk modulus have been plotted with pressure range 0–121 GPa in Fig. 3. It is obvious from the figure that $C_{11}$ varies largely under the effect of pressure as compared with the variations in the $C_{12}$ and $C_{44}$. Since the elastic constant $C_{11}$ represents elasticity in length. A longitudinal strain produces a change in $C_{11}$. The elastic constants $C_{12}$ and $C_{44}$ are related to the elasticity in shape, which is a shear constant. A transverse strain causes a change in shape without a change in volume. Therefore, $C_{12}$ and $C_{44}$ are

less sensitive of pressure as compared with $C_{11}$. $C_{44}$ decreases with increase of the pressure while the bulk modulus of CdO increases with increase of the pressure. In Fig. 3 line+solid squares represent the present values and line+solid triangles represent the data reported by Peng et al. [15]. Present results show the same trend as reported by plane-wave pseudopotential density functional theory.

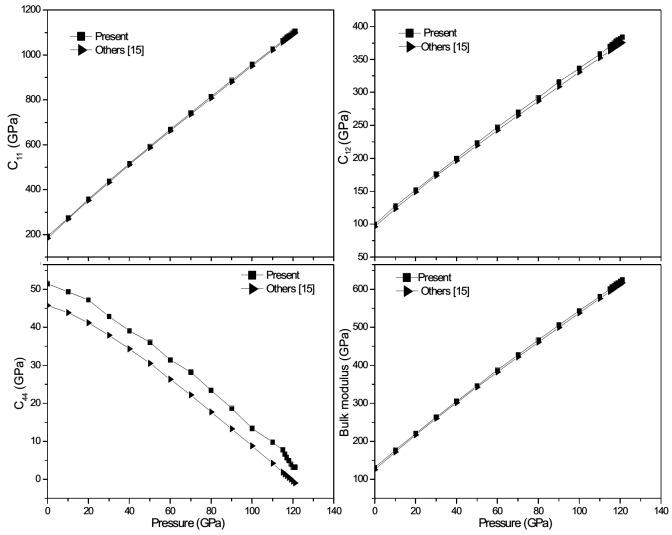


Fig. 3. Variation of SOEC's and bulk modulus with pressure.

It is known that even the cubic crystal which has isotropic structure, has elastic anisotropy as a result of a fourth rank tensor property of elasticity. The elastic anisotropic parameter of cadmium oxide has been calculated, using the following relation:

$$A = \frac{2C_{44}}{C_{11} - C_{12}}. \tag{13}$$

The calculated values of anisotropic parameter $A$ of CdO have been depicted in Table V with various pressures. For an isotropic crystal the value of $A$ is 1. For any values smaller or larger than 1, there was indicated the presence of anisotropy.

The shear modulus $G$ can be defined by the following equation:

$$G = (G_{\mathrm{V}} + G_{\mathrm{R}})/2, \tag{14}$$

where $G_{\mathrm{V}} = (2C + 3C_{44})/5$, $G_{\mathrm{R}} = 15(6/C + 9/C_{44})^{-1}$, where $C = (C_{11} - C_{12})/2$. $G_{\mathrm{V}}$ is the Voigt shear modulus and $G_{\mathrm{R}}$ is the Reuss shear modulus.

We have also calculated the Young modulus $Y$, which is related to the bulk modulus $B$ and the shear modulus $G$ by the following equation [23]:

$$Y = 9BG(3B + G). \tag{15}$$

Our calculated values of anisotropy $A$, shear modulus $G$, Young's modulus $Y$ of cadmium oxide at zero pressure are also listed in Table V. These values of combination of elastic constants are compared with first principle calculations performed by Peng et al. [15].

TABLE V

Calculated values of shear modulus ($G$), Young modulus ($Y$), anisotropy ($A$), Poison ratio ($\sigma$) and Debye temperature ($\theta_{\mathrm{D}}$) for CdO.

| $P$ | $G$ | $Y$ | $A$ | $\sigma$ |
|---|---|---|---|---|
| 0 (present) | 49.43 | 131.70 | 1.108 | 0.332 |
| (others) | 45.06 | 120.70 | 1.041 | 0.339 |
| 10 (present) | 58.87 | 174.07 | 0.674 | 0.335 |
| (others) | 53.90 | 146.44 | 0.600 | 0.358 |
| 20 (present) | 69.57 | 188.85 | 0.457 | 0.357 |
| (others) | 59.73 | 164.11 | 0.405 | 0.374 |
| 30 (present) | 78.35 | 213.88 | 0.325 | 0.364 |
| (others) | 63.82 | 176.97 | 0.292 | 0.387 |
| 40 (present) | 86.90 | 238.12 | 0.246 | 0.370 |
| (others) | 66.74 | 186.45 | 0.218 | 0.397 |
| 50 (present) | 95.37 | 262.07 | 0.195 | 0.373 |
| (others) | 68.88 | 193.66 | 0.166 | 0.406 |
| 60 (present) | 103.05 | 283.97 | 0.149 | 0.377 |
| (others) | 70.15 | 198.34 | 0.126 | 0.414 |
| 70 (present) | 111.27 | 307.13 | 0.119 | 0.380 |
| (others) | 70.98 | 201.64 | 0.094 | 0.420 |
| 80 (present) | 118.63 | 328.08 | 0.089 | 0.382 |
| (others) | 71.61 | 204.26 | 0.068 | 0.426 |
| 90 (present) | 125.37 | 347.41 | 0.065 | 0.385 |
| (others) | 71.88 | 205.77 | 0.047 | 0.431 |
| 100 (present) | 132.18 | 366.81 | 0.043 | 0.387 |
| (others) | 71.88 | 206.43 | 0.028 | 0.436 |
| 110 (present) | 139.74 | 388.12 | 0.029 | 0.388 |
| (others) | 71.65 | 206.40 | 0.013 | 0.440 |
| 115 (present) | 143.29 | 398.22 | 0.022 | 0.389 |
| (others) | 71.50 | 206.24 | 0.005 | 0.442 |
| 116 (present) | 142.94 | 397.52 | 0.014 | 0.390 |
| (others) | 71.46 | 206.17 | 0.004 | 0.443 |
| 117 (present) | 143.22 | 398.45 | 0.012 | 0.391 |
| (others) | 71.40 | 206.06 | 0.003 | 0.443 |
| 118 (present) | 143.42 | 399.17 | 0.008 | 0.391 |
| (others) | 71.35 | 205.97 | 0.001 | 0.443 |
| 119 (present) | 144.08 | 401.03 | 0.007 | 0.391 |
| (others) | 71.33 | 205.95 | 3E−5 | 0.444 |
| 120 (present) | 144.61 | 402.56 | 0.004 | 0.391 |
| (others) | 71.16 | 205.51 | −0.002 | 0.444 |
| 121 (present) | 144.99 | 403.73 | 0.002 | 0.392 |
| (others) | 71.14 | 205.53 | −0.003 | 0.444 |

Others — Ref. [15]

The Poisson ratio of a material influences the speed of propagation and reflection of stress waves. The Poisson ratio is an important property to know the properties of compounds. The Poisson ratio ($\sigma$) of present oxide have been calculated, the expression of $\sigma$ can be given in the following form:

$$\sigma = \frac{3B - 2G}{6B + 2G}. \tag{16}$$

As discussed above Poisson's ratio deals with the way of stretching or compressing an object in one direction, it

causes to compress or stretch in the other direction. The ratio measures the extent of this effect in a particular substance. The Poisson ratio has two limits: it must be greater than $-1$, and less than or equal to 0.5. The calculated values of the Poisson ratio $\sigma$ for CdO are given in Table VI and they are in abovementioned limit. Our values of Poisson's ratio for CdO at different pressures are compared with plane-wave pseudopotential density functional theory method [15]. Present results show the same trend as reported by Peng et al. [15].

TABLE VI

Calculated values of sound velocity (in km/s) and Debye temperature ($\theta_{\rm D}$) in K for CdO.

| $P$ | $v_{\rm l}$ | $v_{\rm t}$ | $v_{\rm m}$ | $\theta_{\rm D}$ |
|---|---|---|---|---|
| 0 (present) | 5.112 | 3.012 | | 388.45 |
| (others) | 4.902 | 2.417 | 2.714 | 413.920[a], 336.5[b] |
| 10 (present) | 5.503 | 3.378 | | 417.59 |
| (others) | 5.439 | 2.556 | 2.876 | 448.644[a], 364.9[b] |
| 20 (present) | 5.924 | 3.654 | | 436.87 |
| (others) | 5.837 | 2.620 | 2.955 | 468.938[a], 381.7[b] |
| 30 (present) | 6.221 | 3.706 | | 452.32 |
| (others) | 6.169 | 2.654 | 2.999 | 482.623[a], 392.5[b] |
| 40 (present) | 6.536 | 3.273 | | 465.96 |
| (others) | 6.453 | 2.664 | 3.015 | 490.982[a], 399.5[b] |
| 50 (present) | 6.722 | 3.391 | | 476.13 |
| (others) | 6.694 | 2.664 | 3.018 | 496.569[a], 404.3[b] |
| 60 (present) | 6.999 | 3.397 | | 484.37 |
| (others) | 6.908 | 2.653 | 3.009 | 499.645[a], 406.6[b] |
| 70 (present) | 7.198 | 3.4 | | 491.45 |
| (others) | 7.120 | 2.637 | 2.993 | 501.185[a], 407.7[b] |
| 80 (present) | 7.383 | | | 496.58 |
| (others) | 7.298 | 2.617 | 2.973 | 501.582[a], 408.2[b] |
| 90.31 (present) | 7.573 | | | 503.76 |
| (others) | 7.476 | 2.595 | 2.950 | 501.244[a], 407.9[b] |
| 100 (present) | 7.846 | | | 514.23 |
| (others) | 7.762 | 3.126 | 3.540 | 618.916[a], 406.8[b] |
| 105 (present) | 7.925 | | | 519.47 |
| (others) | 7.876 | 3.186 | 3.608 | 632.580[a] |
| 110 (present) | 8.097 | | | 524.75 |
| (others) | 7.983 | 3.239 | 3.668 | 644.923[a], 405.2[b] |
| 120 (present) | 8.286 | | | 533.61 |
| (others) | 8.187 | 3.341 | 3.782 | 668.668[a], 402.8[b] |
| 130 (present) | 8.475 | | | 541.36 |
| (others) | 8.380 | 3.437 | 3.890 | 691.338[a] |
| 140 (present) | 8.637 | | | 549.84 |
| (others) | 8.563 | 3.526 | 3.990 | 712.526[a] |
| 150 (present) | 8.842 | | | 557.19 |
| (others) | 8.737 | 3.611 | 4.086 | 732.977[a] |

[a] Ref. [13], [b] Ref. [15]

The values of shear modulus ($G$), Young's modulus ($Y$), anisotropy ($A$) and Poisson's ratio ($\sigma$) have been plotted with pressure in Fig. 4. Present results have been compared for all these values with plane-wave pseudopotential density functional theory method reported by Peng et al. [15]. It is apparent from Fig. 4 that the values of shear modulus, Young's modulus and Poisson's ratio increase with pressure at the same time as the values of anisotropy decrease with increasing the pressure. In Fig. 4 line+solid squares represent the present values and line+solid triangles represent the plane-wave pseudopotential density functional data [15]. Present results demonstrate almost similar behaviour as accounted by Peng et al. [15] except from $G$ and $Y$. The plot of other [15] shear modulus and Young's modulus increases as a curved form, while our plot increases linearly with pressure.

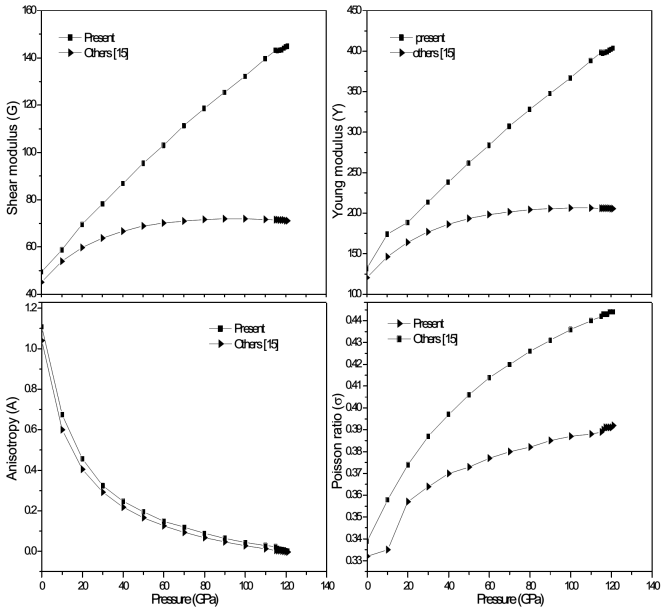


Fig. 4. Variation of shear modulus ($G$), Young's modulus ($Y$), anisotropy ($A$) and Poisson's ratio ($\sigma$) with pressure.

The basic material properties, which are of interest in many manufacturing and research applications, can be determined quickly and easily through computations based on sound velocities. Sound velocity can be easily measured using ultrasonic pulse-echo techniques. In addition, to study the thermodynamic properties of these compounds the average wave velocity $v_{\rm m}$ have been calculated on the lines of Guo et al. [29]. For calculating the average wave velocity $v_{\rm m}$ the expressions are

$$v_{\rm m} = \left[\frac{1}{3}\left(\frac{2}{v_{\rm t}^3} + \frac{1}{v_{\rm l}^3}\right)\right]^{-1/3}, \tag{17}$$

where $v_{\rm l}$ and $v_{\rm t}$ are the longitudinal and the transverse elastic wave velocities, respectively, which are obtained from Navier's equation in the following forms:

$$v_{\mathrm{l}} = \sqrt{\frac{3B + 4G}{3\rho_{\mathrm{D}}}}, \tag{18}$$

$$v_{\mathrm{t}} = \sqrt{\frac{G}{\rho_{\mathrm{D}}}}, \tag{19}$$

where $G$ is the shear modulus, $B$ is the bulk modulus, and $\rho_{\mathrm{D}}$ is the density. The calculated values of longitudinal, transverse and average wave velocities are given in Table V at various pressures. Due to the unavailability of the experimental values of average wave velocities of CdO, we could not compare our results. The average wave velocities of CdO are compared with plane-wave pseudopotential density functional theory method with pressure range 0–150 GPa performed by Peng et al. [15]. We have plotted the longitudinal elastic wave velocity ($v_{\mathrm{l}}$) with pressure in Fig. 6. This variation of longitudinal elastic wave velocity has been compared with density functional theory, using the pseudopotential plane--wave method performed by Li et al. [13]. It is obvious from Fig. 6 that our values of $v_{\mathrm{l}}$ increases with increasing the pressure throughout the pressure range. This plot demonstrates the same behaviour as reported by Li et al. [13].

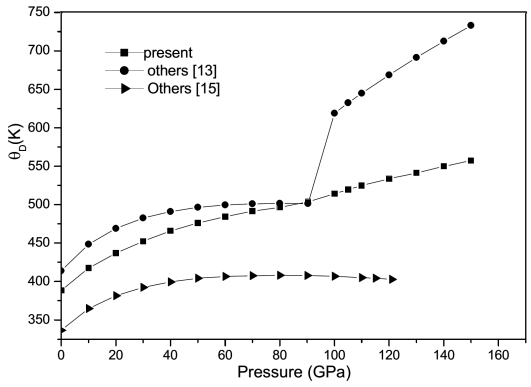


Fig. 5. Variation of Debye temperature with pressure for CdO.

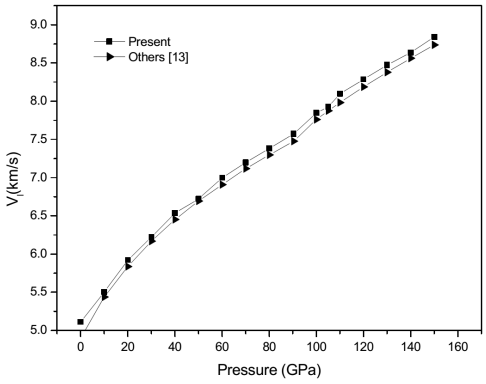


Fig. 6. Variation of the longitudinal elastic wave velocity ($v_{\mathrm{l}}$) with pressure.

With the knowledge of molecular force constant ($f$) and the reduced mass ($\mu$) of the cadmium oxide crystal the Debye temperature of CdO has been calculated. The detailed expressions are given in our earlier paper [21–23]. The frequency with the knowledge of the reduced mass ($\mu$) of the CdO is as follows:

$$\nu_0 = \frac{1}{2\pi}\left(\frac{f}{\mu}\right)^{1/2}. \tag{20}$$

This frequency gives us the Debye temperature

$$\theta_{\mathrm{D}} = \frac{h\nu_0}{k}, \tag{21}$$

with $h$ and $k$ as the Planck and Boltzmann constants, respectively.

Also, thermophysical properties of CdO have also been computed. The thermophysical properties provide us the interesting information about the substance. The Debye characteristic temperature $\theta_{\mathrm{D}}$ reflects its structure stability, the strength of bonds between its separate elements, structure defects availability, and its density. The calculated values of the Debye temperatures have been listed in Table VI at different pressures. Due to the lack of experimental data, we could compare them with plane-wave pseudopotential density functional theory method with pressure range 0–150 GPa performed by Peng et al. [15] and first principle calculations performed by Li et al. [13].

The variation of the Debye temperatures ($\theta_{\mathrm{D}}$) with pressure has been plotted in Fig. 5. This variation has been compared with density functional theory (DFT) and first principle calculations in Fig. 5. It is obvious from the figure that our values of $\theta_{\mathrm{D}}$ increases with increase of the pressure same as first principle calculations performed by Li et al. [13]. While according to plane-wave pseudopotential DFT method performed by Peng et al. [15] the variation tendency of $\theta_{\mathrm{D}}$ is to similar some extent and there is a sudden increase in $\theta_{\mathrm{D}}$ at pressure 85 GPa.

In view of overall estimation it is clear that the present results are close to available experimental data. The accomplishment attained in the present investigation can be ascribed to the inclusion of charge transfer (or three--body) and zero point energy effect.

Ultimately, it may be concluded that the present EIP model has successfully predicted the compression curves and phase diagrams giving the phase transition pressures, associated volume collapses, elastic and thermodynamical properties correctly for CdO. The inclusion of three body interactions with zero point energy effect has improved the prediction of phase transition pressures over that obtained from the two-body potential and TBI without zero point energy.

## References

[1] M.A. Hasse, L. Qui, J.M. Depuydt, H. Luo, N. Samarth, *Phys. Lett.* **59**, 1273 (1991).

[2] J. Gaines, R. Drenten, K. Haberen, W. Marshall, P.M. Mensz, J. Petruzzello, *Phys. Lett.* **62**, 2462 (1993).

[3] M. Fuchs, M. Bockstede, E. Pehlke, M. Scheffler, *Phys. Rev. B* **57**, 2134 (1998).

[4] M. Ristric, S. Popovic, S. Music, *Mater. Lett.* **58**, 2494 (2004).

[5] K. Gurumurugan, D. Mangalaraj, *Cryst. Growth* **147**, 355 (1995).

[6] A. Schleife, F. Fuchs, J. Furthmuller, F. Bechstedt, *Phys. Rev. B* **73**, 245212 (2006).

[7] J.E. Jaffe, J.A. Snyder, Z. Lin, A.C. Hess, *Phys. Rev. B* **62**, 1660 (2000).

[8] H. Liu, H. Mao, M. Somayazulu, Y. Ding, Y. Meng, D. Häusermann, *Phys. Rev. B* **70**, 094114 (2004).

[9] F.D. Murnagham, *Proc. Natl. Acad. Sci. USA* **30**, 244 (1994).

[10] R.J. Guerrero-Moreno, N. Takeuchi, *Phys. Rev. B* **66**, 205205 (2002).

[11] F. Peng, D. Chen, H. Fu, X. Cheng, *phys. status solidi b* **246**, 71 (2009).

[12] A.A. Dakhel, *J. Alloys Comp.* **475**, 51 (2009); *Sol. En.* **83**, 934 (2009); *Opt. Mater.* **31**, 691 (2009); *Thin Solid Films* **518**, 1712 (2010).

[13] G.-Q. Li, C. Lu, X.-Q. Yang, S.-W. Xiao, A.-H. Wang, L. Wang, X.-M. Tan, *High Press. Res.* **30**, 679 (2010).

[14] M.S. Dhaka, U. Paliwal, G. Sharma, M.C. Mishra, K.B. Joshi, R.K. Kothari, B.K. Sharma, *J. Alloys Comp.* **501**, 136 (2010).

[15] F. Peng, Q. Liu, H.Z. Fu, X.D. Yang, *Solid State Commun.* **148**, 6 (2008).

[16] R.K. Singh, S. Singh, *Phys. Rev. B* **39**, 671 (1989); *Phase Transit.* **15**, 127 (1997).

[17] R.K. Singh, S. Singh, *Phys. Rev. B* **45**, 1019 (1992).

[18] S. Singh, R.K Singh, R. Rai, B.P. Singh, *J. Phys. Soc. Jpn.* **68**, 1269 (1999).

[19] P. Bhardwaj, S. Singh, N.K. Gaur, *J. Centr. Europ. J. Phys.* **6**, 223 (2008).

[20] P. Bhardwaj, S. Singh, N.K. Gaur, *Mater. Res. Bull.* **44**, 1366 (2009).

[21] P. Bhardwaj, S. Singh, *Physica B* **406**, 1615 (2011).

[22] P. Bhardwaj, S. Singh, *phys. status solidi b* **249**, 38 (2012).

[23] P. Bhardwaj, S. Singh, *Mater. Chem. Phys.* **125**, 440 (2011).

[24] P.O. Lowdin, *Adv. Phys.* **75**, 1 (1932); *J. Chem. Phys.* **18**, 113 (1961).

[25] S.O. Lundqvist, *Ark. Fys. (Sweden)* **12**, 365 (1958).

[26] D.W. Hafemeister, H.F. Flygare, *J. Chem. Phys.* **43**, 795 (1965).

[27] M.P. Tosi, F.G. Fumi, *J. Phys. Chem. Solids* **23**, 359 (1962); M.P. Tosi, *Solid State Phys.* **16**, 1 (1964).

[28] R.K. Singh, *Phys. Rep.* **85**, 259 (1982).

[29] Y.-D. Guo, Z.-J. Yang, Q.-H. Gao, Z.-J. Liu, W. Dai, *J. Phys., Condens. Matter* **20**, 115203 (2008).